Solid Freeform Fabrication 2017: Proceedings of the 28th Annual International Solid Freeform Fabrication Symposium – An Additive Manufacturing Conference
Reviewed Paper

Modeling of Low One-photon Polymerization for 3D printing of UV-curable Silicones

Dong Sung (Danny) Kim[1], Jakkrit Suriboot[2], Melissa Grunlan[2], Bruce L. Tai[1,*]
Department of Mechanical Engineering[1]
Department of Biomedical Engineering[2]
Texas A&M University

Keywords: additive manufacturing; silicone 3D printing; low one-photon polymerization

Abstract

Low-one photon polymerization (LOPP) enables an in-liquid curing to suspend a soft silicone object in the vat without mechanical disturbance. LOPP requires a low-absorbance wavelength and a great gradient light beam to achieve the desired curing. To further control the process for 3D printing, this research aims to model LOPP behaviors of a custom-made UV-curable silicone system based on Gaussian beam and Beer-Lambert law. A methyl acrylate-based silicone was specifically formulated to pair with a 375 nm UV light and high numerical aperture lens in this work. The silicone was established with critical exposure and penetration depth by a modified "windowpane" test. The comparison results between the model and LOPP tests showed a consistent trend of polymerization. This model suggested a large penetration depth and smaller critical exposure to achieve an ideal LOPP-based printing.

1. Introduction

Silicones have broad applications in bio-medical research [1], soft robotics [2], clinical simulation [3], and many others due to the fact that they are biocompatible, corrosion resistive, mechanically strong, and chemically stable under a high temperature. Molding is the most common technique to fabricate silicones into functional products. However, physical limitations can make the manufacturing process complex for enclosed cavities, internal channels, and high-aspect-ratio features. Additive manufacturing (AM) of silicones opens a new paradigm for silicone engineered applications by solving these issues. A few researchers and commercial products have studied 3D printing silicones with extrusion-based AM techniques. Jin et al. presented an extrusion-based process with a humidity cured silicone on an FDM machine platform [4]. Commercial products like Bioplotter (Envision Tech, Dearborn, MI) and Picsima (Fripp design and research, Rotterdam, United Kingdom) use a two-part silicone and syringe extruder to create 3D geometries; WACKER (Munich, Germany) uses UV-curable silicone and the drop-on-demand technology for printing. However, it is still technically challenging to print silicones in to complex shapes because of the deformation resulting from the low stiffness and the lack of support structure. There is currently no compatible support material for silicones.

Kim et al. [5] proposed and demonstrated an in-liquid printing process for this challenge using a hydrostatic environment as support and eliminating the nozzle (extrusion method) to avoid

disturbing the fluid and cured part. This idea can be achieved by UV-curable silicones via the low-one photon polymerization (LOPP) phenomenon. Compared to the regular one-photon polymerization (OPP) used in stereolithography (SLA) [6], LOPP can create a restricted curing point inside the liquid resin around the focal spot [7]. By adjusting the focal point, the curing can occur at anywhere in the three-dimensional space rather than on a 2D plane in SLA. This way provides more degrees of freedom in printing path design to avoid isolated pieces or overhanging structures.

On the other hand, however, it is difficult to control LOPP in terms of time, location, and voxel size. The applicable wavelength range and light intensity are generally narrow and can vary significantly from one photopolymer to another. LOPP is also dependent on the irradiance created by the optical setup. For this reason, the objective of this study is to develop a process model to understand the significance of different process parameters and material properties, and thus enable a process control for silicone 3D printing. The LOPP model can be modified from existing SLA modeling techniques [8] by further considering the gradient and attenuated irradiance.

In this paper, the modeling concept is first introduced and followed by the experimental study to compare the results and validate the model. A material selection guideline for LOPP will be discussed at the end as well as the current model limitations for improvement.

2. LOPP Model Setup

This section presents step-by-step procedures to create the model and the methods to determine the model parameters.

2.1. Model construction

The LOPP model consists of two parts, irradiance model and curing model. The irradiance model describes the energy distribution from the light source inside the liquid resin by considering the UV beam profile and the effect of attenuation as shown in Fig. 1. The curing model predicts the time at which a unit volume is cured inside the liquid resin by setting a threshold value.

The energy distribution in the irradiance model is determined by the beam gradient and attenuation. The collimated light source is converged by a focusing lens to reach the maximum at the focal spot along the axial direction and then diversifies again. Due to the attenuation in the liquid resin, the convergence and divergence are not linear along the depth. To construct this model, first, the original collimated light source is assumed to be a Gaussian distribution in the radial direction, as expressed by Eq. (1) and Fig. 2 (a).

$$H(x,y) = H_0 \cdot e^{-2x^2/{W_0}^2} e^{-2y^2/{W_0}^2} \qquad (1)$$

where W_0 is the radius of the Gaussian beam and H_0 is the maximum irradiance based on the power of the light source P_L, so that $H_0 = \frac{2P_L}{\pi {W_0}^2}$. As the beam converges towards the focal spot, the beam

diameter changes as well (denoted by W_z); hence, Eq. (1) can be generalized to Eq. (2) while the total beam power remains the same, such that $H_z = \frac{2P_L}{\pi {W_z}^2}$.

$$H(x,y) = H_z \cdot e^{-2x^2/{W_z}^2} e^{-2y^2/{W_z}^2} \qquad (2)$$

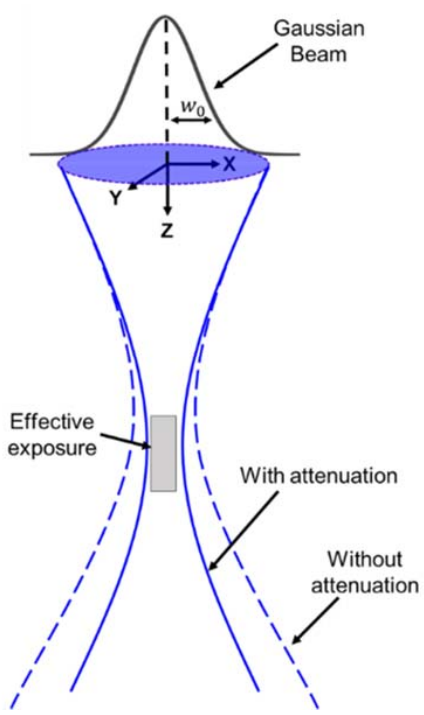

Figure 1: Schematic of the irradiance model in LOPP

The beam radius W_z is assumed to linearly decrease from W_0 to the focal spot, such that

$$W_z = W_0 - (tan\theta) \cdot z, \; z \leq BFL \qquad (3)$$

where $tan\theta$ is determined by the numerical aperture (NA) and refractive index (n) of the focusing lens, *i.e.,* $NA = n\ sin\theta$. The beam profile and irradiance field then change to Fig. 2 (b). It is important to note that the lens with a larger NA has a greater beam gradient but also a shorter focal length. The maximum NA is 1 in the air.

The attenuation is a consequence of light absorption by the photoinitiators in the photopolymer, which can be described as an exponential decade along the depth by Beer-Lambert law. This further transforms Eq. (2) to the following form,

$$H(x,y,z) = \frac{2P_L}{\pi {W_z}^2} \cdot e^{-2x^2/{W_z}^2} e^{-2y^2/{W_z}^2} e^{-Z/D_p} \qquad (4)$$

where D_p is the penetration depth of the photopolymer at which the irradiance decades to *1/e* (about 37%). Noted that D_p is a material property, which is an attenuation coefficient of the resin under a certain wavelength. Due to the attenuation, the beam profile and irradiance become asymmetric to the focal spot, as shown in Fig. 2 (c). Having derived a complete irradiance function, the total exposure E within the irradiated domain can be calculated by multiplying the exposure time (t), such that

$$E(x,y,z,t) = \frac{2P_L}{\pi {W_z}^2} \cdot t \cdot e^{-2x^2/{W_z}^2} e^{-2y^2/{W_z}^2} e^{-Z/D_p} \quad (5)$$

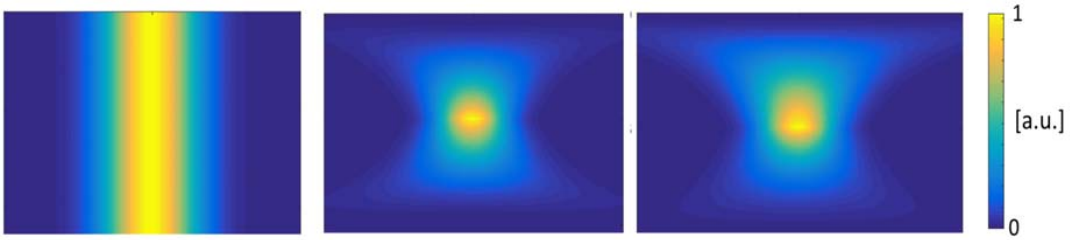

(a) (b) (c)

Figure 2: Irradiance fields generated by (a) uniform beam without the attenuation, (b) gradient beam without the attenuation, and (c) gradient beam with the attenuation.

Lastly, assuming a threshold exposure (E_c) at which the photopolymer begins to cure, the curing profile can be identified by equating Eq. (5) to E_c at each time step. Numerically, the curing volume can be computed by counting the number of elements in the gridded domain that have the total exposure equal or larger than E_c. Noted this method does not consider the polymerization kinetics; the threshold value needs to be experimentally determined.

2.2. Parameters and material properties

In this study, a methyl acrylate-based silicone photopolymer is formulated in-house for a controllable property. It is important to note that this is a different silicone system from the other experimental study conducted by Kim et al. [9, 10]. Fig. 3 shows the absorbance spectrum of the photopolymer measured by a U-4100 Hitachi spectrophotometer (Tokyo, Japan). The wavelength of 375 nm was chosen to create the LOPP effect because of the low absorbance rate (0.011) and the availability of optical components.

According to Section 2.1, the model parameters include laser power P_L, beam radius W_0, penetration depth D_p, critical exposure E_c, and numerical aperture NA. The optical parameters (P_L, W_0, and D_p) are given. The material properties, D_p and E_c, are wavelength-dependent, so they are determined experimentally using the "windowpane" test [11].

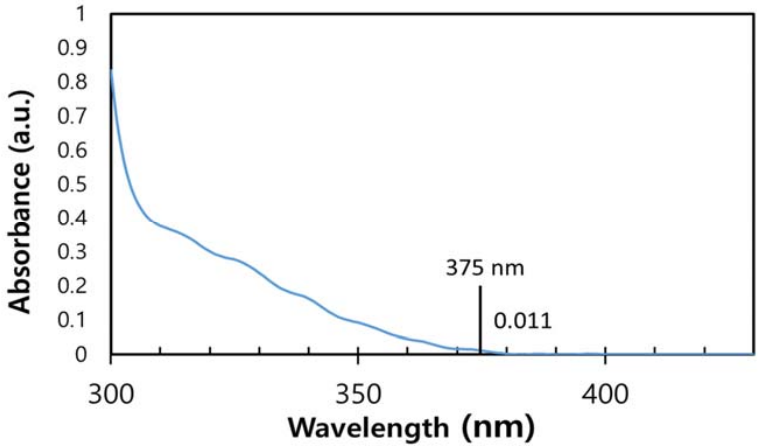

Figure 3: Absorbance spectrum of the tested UV-curable silicone

In this test, a resin container is filled with the photopolymer and covered with a slide glass of 0.15 mm thick. The beam power is set at 0.76 mW and the beam diameter is 1.6 mm. A single-wavelength and uniform beam generated by the collimating lens and the band pass filter is irradiated through the slide glass from the top as shown in Fig. 5. The silicone starts to cure downward from the slide class and form a conical shape over time due to the Gaussian beam. The depth of the cured part is denoted by C_d, which is a function of time. This depth is measured by optical images with 0.05 mm resolution (per pixel).

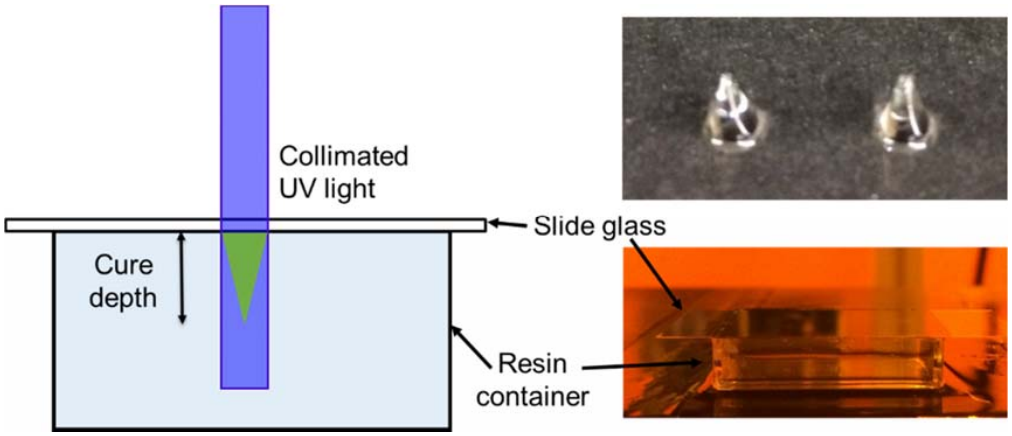

Figure 5: Schematic diagram and pictures of the windowpane test.

Given the cure depth at a certain exposure, the penetration depth D_p and critical exposure E_c can be obtained by modifying Eq. (5) by replacing the gradient beam and setting x and y to be zero for the maximum exposure spot (at the center or the conical shape), such that

$$E_c = \frac{2P_L}{\pi {W_0}^2} \cdot t \cdot e^{-C_d/D_p} \qquad (6)$$

By sorting out Eq. (6), C_d can be mathematically determined by Eq. (7) below by drawing a linear relationship between all measured depths and the logarithms of the total exposure at various exposure times. The line slope is D_p; the intercept of the line gives the logarithm of the critical exposure E_c. This linear relation is also called "working curve" in the windowpane test.

$$C_d = D_p \cdot \left[ln(\frac{2 \cdot P_L}{\pi \cdot {w_0}^2} \cdot t) - ln(E_c) \right] \qquad (7)$$

Seven testing points (exposure times) were performed in this task to create a working curve in Fig. 6, where D_p = 2.24 mm and E_c = 2.09 mJ/mm^2 were determined for this particular UV-curable silicone at 375 nm.

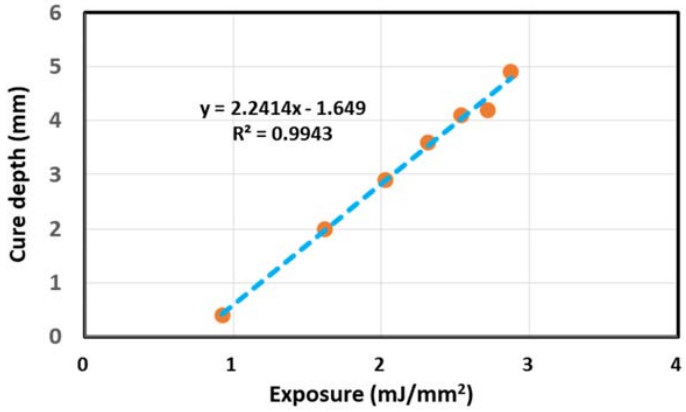

Figure 6: Working curve for the selected UV-curable silicone

3. Experiments for Model Validation

This section describes the experimental study to validate the model and the comparison results.

3.1. Experimental setup and method

The experimental setup is composed of a UV lamp system (OmniCure S2000, Excelitas Technologies Corp., Waltham, MA) an optical lens array (Edmund Optics Inc., Barrington, NJ) as shown in Fig. 7. The whole setup is covered by amber plates to block ambient UV light. The lamp system has a full spectrum ranging from 250 nm to 650 nm. The optical lens array consists of aspheric lenses, a 375 nm band pass filter, and iris diaphragms. Two aspheric lenses are used to collimate and focus the beam, respectively. The second aspheric lens used for focusing has the numerical aperture of 1 and the back focal length (BFL) of 6.9 mm. The band pass filter harvests the 375 nm wavelength from the full spectrum of the lamp system with a resultant power of 0.76 mW. The iris diaphragms are employed to condition the beam profile. An acrylic box is used as the resin container with the external dimensions of 25.4 mm by 25.4 mm by 6.3 mm.

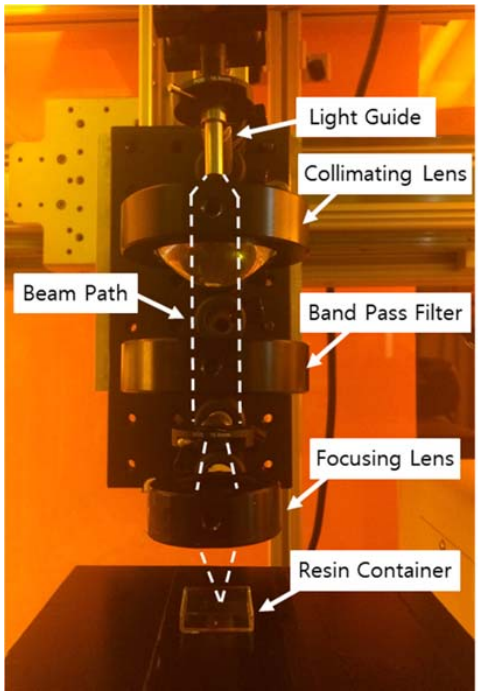

Figure 7. The picture of the optical lens array

The single-spot test [10] is utilized to quantitatively validate the LOPP process. The liquid silicone photopolymer fully fills the container. The UV light is irradiated and focused on the bottom of the container as shown in Fig. 8. In an ideal LOPP condition, a pillar (not necessarily cylindrical) could grow from the focal spot (the bottom of the container) towards the liquid surface over time. If LOPP does not exist due to a high power or high-absorbance wavelength, the pillar will form immediately throughout the depth. Since it is not possible to monitor and measure the pillar height in real-time during the exposure test, pillars with various exposures are generated as discrete data points to draw the relationship. The exposure times are from 1 min to 15 mins with an interval of 1 min. A total of 15 data points are tested. The test is repeated three times to ensure the repeatability. The pillar height is measured by optical images with 0.05 mm resolution.

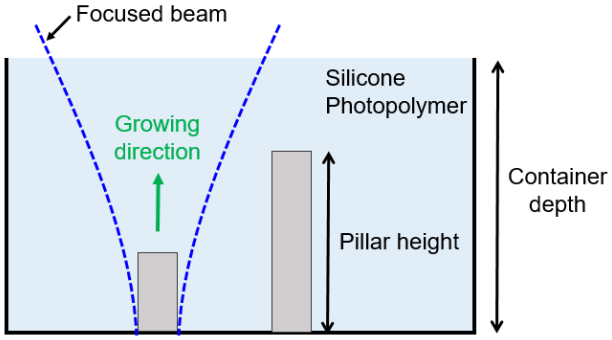

Figure 8: Schematic diagram of the single-spot test

3.2. Results

Fig. 9 shows the result of the pillar height against exposure time and the model-predicted curve. Both experiment and simulation results show the LOPP phenomenon. The three experimental tests show a consistent trend and a steady slope of pillar growing that clearly indicates LOPP. No cured part can be measured from 1 min to 4 mins due to lack of exposure or losing the small pillars. The first curing point appears at 5 mins and grows gradually as the exposure time increases. The pillar has reached the resin surface after 9 mins of exposure. In comparison, the LOPP model shows a slow growth from 1.4 mins to about 4 mins and turns into a rapid growth after 5.6 mins. The small three windows in Fig. 9 illustrate the results at 2.1, 4.2, and 5.8 mins of exposure. It can be seen that the polymerization begins from the liquid surface after 5.6 mins, thereby accelerating the pillar formation throughout the resin depth. The model-predicted pillar growth occurs much earlier between 1 to 2 mins, but the mid-range profile (5 to 6 mins) is similar to that of the experiment. The aforementioned discrepancies could be due to both model and experiment limitations, which will be discussed in the next section.

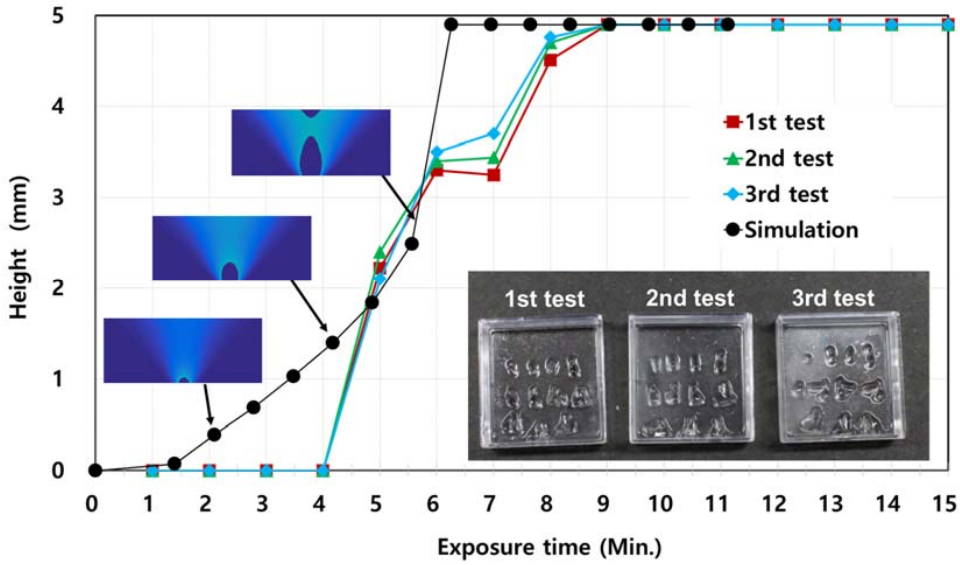

Figure 9: Pillar height vs. exposure time and the results from the single-spot test and model simulation.

4. Discussion

This section explains the possible error sources contributed to the mismatch; this section also discusses the effects of silicone optical properties to the LOPP phenomenon using the current model.

4.1. Model and experiment limitations

One major challenge in the experiment is to measure the pillar size. Since the silicone is transparent, the uncured resin needs to be drained to make pillars visible and measurable. This

procedure can potentially remove the small pillars that have not sufficiently adhered to the container base. Therefore, there is a possibility of missing small parts generated between 1 to 4 mins of exposure; it could also be true that nothing is formed. The second issue is the power stability at the level of less than 1 mW when the system harvests the 375 nm wavelength from the full spectrum. The instability could cause the growth retardation such as the growth between 6 and 7 mins of exposure.

On the model side, the effect of the refractive index is not considered since the data sheet provides the number (about 1.5) only from the visible light (via a standard measurement device). Measuring 375 nm would require a special device or setup. The refractive index could change when the wavelength decreases. This leads to a different gradient (Eq. (3)) in the model, thus different curing conditions [6, 12]. Another limitation is the curing model using a critical exposure E_c without considering the material kinetics, such as initiation, propagation, and termination. The growth retardation could result from progress rates of the three steps.

4.2. Material effects

Using this preliminary model, the basic effects of the polymer's optical properties (penetration depth D_p and critical exposure E_c) on LOPP can be studied to aid future material synthesis and characterization. Two sets of conditions were run with the model. One varys D_p and the other varys E_c Figs. 10 (a) and (b) (top row) show the energy distributions under different penetration depths (2.44 and 1.24 mm).

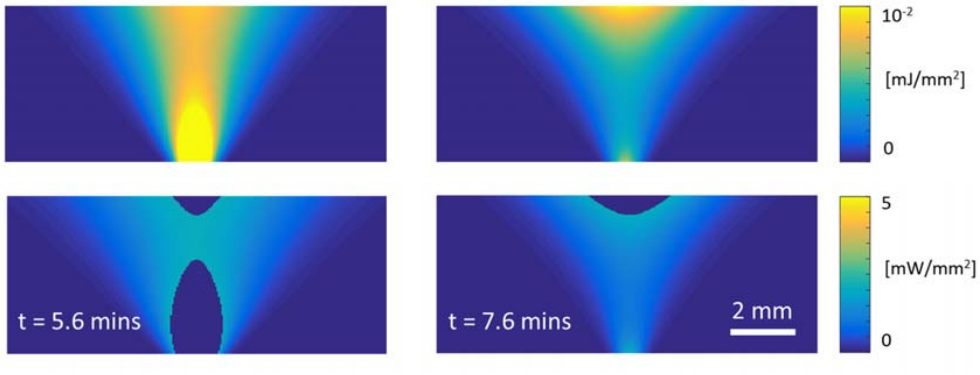

(a) (b)

Figure 10: Irradiance model and curing model with (a) with D_p = 2.24 mm and t = 5.6 mins and (b) with D_p = 1.24 mm and t = 7.6 mins.

Fig. 10 (a) (bottom row) is a snapshot during the pillar growth under the current experimental condition (the same as Fig. 9). The first curing point starts from the focal spot; the second curing point appears from the liquid surface after a certain exposure. Eventually, they meet at the certain point. A smaller penetration depth of 1.24 mm makes the irradiance field fairly different compared to the counterpart. Such distribution leads to a curing point only from the surface. The results suggest that penetration depth is critical to the energy distribution to achieve LOPP. High D_p

produces a higher intensity at the focal spot to enable LOPP, while low D_p makes a higher intensity at the surface. From the material synthesis perspective, a higher D_p can be achieved with a longer wavelength (lower absorbance). The long curing time, as a result of low absorbance, can be offset by a higher concentration of the photoinitiator.

Figure 11 shows the effect of the critical exposure E_c on pillar growth. The penetration depth remains at 2.44 mm in this set of tests, and E_c are 2.09, 2.8 and 3.5 mJ/mm^2, respectively. The dramatic growth of the last points results from the emergence of the second curing point from the resin surface. Overall, as E_c increases, the first curing point appears later and the growing rates decreases. This change is linearly proportional to the critical exposure. This finding shows that E_c is an important parameter to control the time of LOPP.

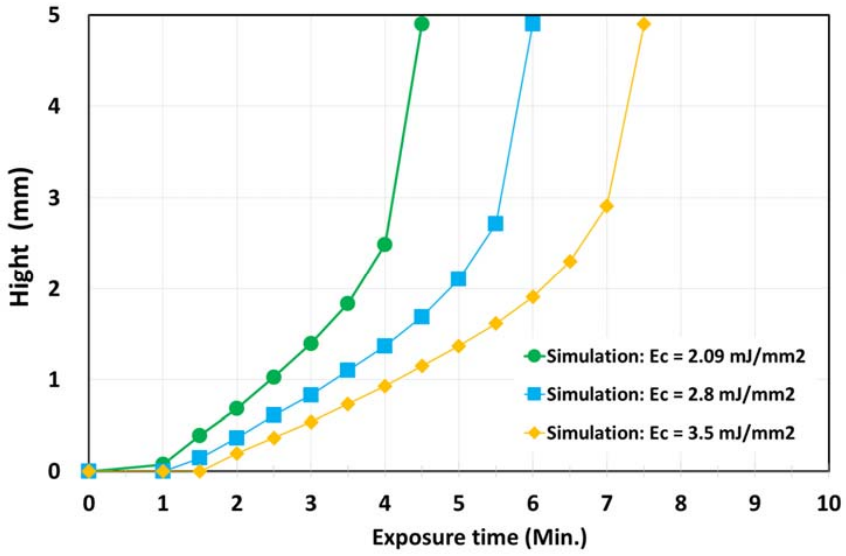

Figure 11: The effect of the critical exposure E_c for the exposure time vs. height.

5. Conclusions

This study develops a simulation model to describe the LOPP behaviors of a UV-curable silicone. Based on the experimental study, the simulation model produces meaningful predictions in terms of the growth trend and time, though they do not completely match. The model suggests that LOPP is sensitive to material parameters - the penetration depth D_p and critical exposure E_c. In particular, D_p can significantly change the irradiance distribution; insufficient D_p can suppress the LOPP despite the gradient beam. The E_c linearly scales the curing rate, and it can control the overall time. In conclusion, the ideal LOPP process can be achieved by creating a largely gradient beam and finding a photopolymer with large D_p and small E_c.

The future work will focus on improving the model accuracy based on the limitations found in this study, including pillar size, small power source, and liquid refractive index under UV light range. The polymer kinetics can be incorporated into the current model to further improve the accuracy.

6. Acknowledgements

This research is partially supported by Los Alamos National Labs and National Science Foundation Grant (#1522877).

7. References

[1] Place, E. S., George, J. H., Williams, C. K., and Stevens, M. M., 2009, "Synthetic polymer scaffolds for tissue engineering," Chemical Society Reviews, 38(4), pp. 1139-1151.

[2] Roche, E. T., Wohlfarth, R., Overvelde, J. T. B., Vasilyev, N. V., Pigula, F. A., Mooney, D. J., Bertoldi, K., and Walsh, C. J., 2014, "A Bioinspired Soft Actuated Material," Advanced Materials, 26(8), pp. 1200-1206.

[3] Laurent, M., Scheer, P., Dejou, J., and Laborde, G., 2008, "Clinical evaluation of the marginal fit of cast crowns – validation of the silicone replica method," Journal of Oral Rehabilitation, 35(2), pp. 116-122.

[4] Jin, Y., Plott, J., and Shih, A., "Extrusion-based additive manufacturing of the moisture-cured silicone elastomer," Proc. The Solid Freeform Fabrication Symposium, pp. 308-318.

[5] Kim, D. S., Kao, Y.-T., and Tai, B. L., 2016, "Hydrostatic 3D-printing for soft material structures using low one-photon polymerization," Manufacturing Letters, 10, pp. 6-9.

[6] Bártolo, P. J., 2011, Stereolithography: materials, processes and applications, Springer Science & Business Media.

[7] Li, Q., Do, M. T., Ledoux-Rak, I., and Lai, N. D., 2013, "Concept for three-dimensional optical addressing by ultralow one-photon absorption method," Optics Letters, 38(22), pp. 4640-4643.

[8] Jacobs, P. F., "Fundamentals of stereolithography," Proc. The Solid Freeform Fabrication Symposium, pp. 196-211.

[9] Kim, D. S., and Tai, B. L., 2016, "Hydrostatic support-free fabrication of three-dimensional soft structures," Journal of Manufacturing Processes, 24, pp. 391-396.

[10] Kim, D. S. D., Thompson, S., Grunlan, M., and Tai, B. L., "Optimization of Low One-photon Polymerization for Hydrostatic 3D Printing of Silicone Material," Proc. The Solid Freeform Fabrication Symposium, pp. 1094-1102.

[11] Jacobs, P. F., 1992, Rapid prototyping & manufacturing: fundamentals of stereolithography, Society of Manufacturing Engineers.

[12] Lahiri, A., 2016, Basic Optics: Principles and Concepts, Elsevier.